Effect of Zinc and Severe Plastic Deformation on Mechanical Properties of AZ61 Magnesium Alloy

Song-Jeng Huang *, Sheng-Yu Wu , Murugan Subramani

Posted Date: 11 March 2024

doi: 10.20944/preprints202403.0603.v1

Keywords: AZ61 Magnesium Alloy; ECAP; heat treatment; Mechanical Properties; Corrosion resistance

Article

Effect of Zinc and Severe Plastic Deformation on Mechanical Properties of AZ61 Magnesium Alloy

Song-Jeng Huang [1,*], Sheng-Yu Wu [2] and Murugan Subramani [2]

[1] Department of Mechanical Engineering, National Taiwan University of Science and Technology (NTUST), Taipei, 10607, Taiwan; shengyou1999@gmail.com (S.-Y.W.); smurugan2594@gmail.com (M.S)

* Correspondence: sgjghuang@mail.ntust.edu.tw (S.-J.H.)

Abstract: This study investigates the effects of Zinc (4wt.%) and severe plastic deformation on the mechanical properties of AZ61 magnesium alloy through the stir-casting process. The severe plastic deformation (equal channel angular pressing (ECAP)) has been done followed by T4 heat treatment. The microstructural examinations revealed that the addition of 4wt.%Zn enhances the uniform distribution of β-phase, contributing to a more uniformly corroded surface in corrosive environments. Additionally, dynamic recrystallization (DRX) significantly reduces the grain size of as-cast alloys after undergoing ECAP. The attained mechanical properties demonstrate that after a single ECAP pass, AZ61 + 4wt.%Zn alloy exhibits optimal yield strength (YS), ultimate compression strength (UCS), and hardness. This research highlights the promising potential of AZ61 + 4wt.%Zn alloy for enhanced mechanical and corrosion-resistant properties, offering valuable insights for applications in diverse engineering fields.

Keywords: AZ61 Magnesium Alloy; ECAP; heat treatment; Mechanical Properties; Corrosion resistance

1. Introduction

In the aerospace, automotive, and green energy industries, the concept of employing large structural components has gained widespread acceptance due to their immense potential in enhancing operational efficiency, reducing carbon dioxide emissions, and achieving light-weighting. The pursuit of these characteristics has driven extensive research and development efforts [1–4]. Magnesium alloys, being the lightest structural metals, are considered a powerful choice for achieving industrial light-weighting. With a density of only two-thirds that of aluminum alloys and one-fourth that of steel, magnesium alloys offer significant advantages in light-weighting.

Furthermore, magnesium alloys possess advantageous features such as high damping for shock absorption, efficient heat dissipation, and recyclability. For example, in the automotive industry, magnesium alloys find application in various components like steering wheels, seat frames, dashboard frames, and gearbox casings [5,6].

Despite these merits, challenges persist in the application of magnesium alloys. Issues such as corrosion resistance and strength need further improvement to meet the application requirements under high-temperature conditions in the automotive engine compartment [7–9]. Additionally, the processing performance of magnesium alloys requires enhancement to replace traditional steel and aluminum materials in a broader range of automotive components [10]. The automotive industry, grappling with the need for increased safety and luxury features, faces the challenge of minimizing overall vehicle weight [11]. Therefore, the development of new magnesium alloy composites and improved magnesium alloy processing techniques is crucial for achieving automotive light-weighting [12,13].

To address these challenges, various strategies have been devised, including alloying, heat treatment, and the application of severe plastic deformation (SPD) [14–16]. Among SPD techniques, equal channel angular pressing (ECAP) has been demonstrated to yield the most significant grain refinement effects in magnesium alloys [15,17]. The ECAP process generates a substantial amount of cumulative strain, playing a crucial role in the microstructure and texture evolution of magnesium

 doi:10.20944/preprints202403.0603.v1

alloys. In the ECAP process, materials are typically preheated to approximately half of their melting point [18], as done in this study at 350°C. Given that magnesium's hexagonal close-packed (HCP) crystal structure has only two independent slip systems at low temperatures, dynamic recrystallization (DRX) becomes crucial for the microstructure and texture evolution of magnesium alloys subjected to ECAP treatment [19,20].

In the initial grains and twin boundaries, new very small grains form in a specific crystallographic orientation due to DRX [21]. Aqeel Abbas et al. (2020) employed AZ91 magnesium alloy as the base material [22], added 1 wt.% tungsten disulfide (WS2) as a reinforcement phase, and used mechanical stirring casting to prepare the composite material. The composite was homogenized at 410°C for 24 hours and annealed at 200°C. The severe plastic deformation process chosen was ECAP, and the results showed that after 4 ECAP passes, the grain size reduced to 0.2 mm, with hardness and tensile yield strength increasing by 20.45% and 103.5%, respectively. Moreover, 4 ECAP passes exhibited the highest ultimate tensile strength of 324.8 MPa.

This study investigates the impact of alloying (increasing Zn content), solution heat treatment (T4 heat treatment), and severe plastic deformation (ECAP) on the strength enhancement of AZ61 magnesium alloy. There is a lack of comprehensive re-search on the combined effects of heat treatment and ECAP on the mechanical properties of AZ61 Mg alloy. Thus, this investigation delves into the microstructure analysis, mechanical properties, and corrosion resistance of both AZ61 alloy and AZ61+4wt.%Zn, considering the influence of heat treatment and ECAP.

2. Materials and Methods

2.1. Materials Preparation

A commercial AZ61 magnesium alloy (mainly composed of Al-5.95% and Zn-0.64%) (Bo Tao Nanotechnology Co., Ltd. Taiwan) served as the matrix component. Zn powder (4 wt.%) (Emperor Chemical Co., Ltd. Taiwan) particles were used as reinforcements.

The composites were produced by a stir casting technique shown in Figure 1. First, the base material and reinforcement were kept into the crucible furnace. When the temperature reaches 400°C, add SF6 + CO2 mixture of gas to avoid buring, and then raise the temperature to 600°C through the Ar gas to prevent the oxidiation, the temperature rises to 760°C and hold the temperature for ten minutes, and then start to stir rapidly for 20 minutes at 250 rpm to make the reinforcement items dispersed, stirring is complete, pull up the plunger to let the molten metal flow into the mold, and then the material can be taken out of the solidification of the natural cooling in the air, and then take out the last casting and shut down the mains power supply [23]. Two different types of cylindrical ingots were prepared using the same method and fabrication process as follows: 1. AZ61 and 2. AZ61 + 4%Zn.

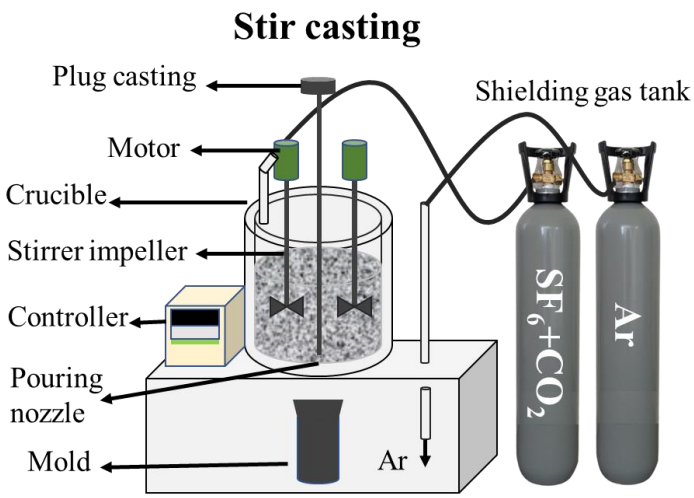

 doi:10.20944/preprints202403.0603.v1

Figure 1. Experimental setup of the stir casting furnace used for the fabrication of the Mg ingot.

Consequently, the ingots were cut into bars measuring 11.5 mm x 11.5 mm x 75 mm, to facilitate subsequent processing steps, including specific heat treatment and Equal Channel Angular Pressing (ECAP) shown in Figure 2.

In this study, we employed the T4 solid solution treatment to fabricate our specimens. Initially, the samples underwent a 24-hour heat treatment at 380°C to achieve a specific solid solution effect. Subsequently, the treated specimens were directly quenched at room temperature to ensure the integrity of the heat treatment process. The purpose of this heat treatment procedure is to tailor the material's crystal structure and mechanical properties to meet the requirements of our research. Followed by the heat treatment, the ECAP fabrication process (Figure 2), was carried out on preheated mold of the ECAP device at 350°C for 40 minutes. Subsequently, a single pass of ECAP was conducted with a channel angle of 120 degrees and a pressing speed of 20 mm/min..

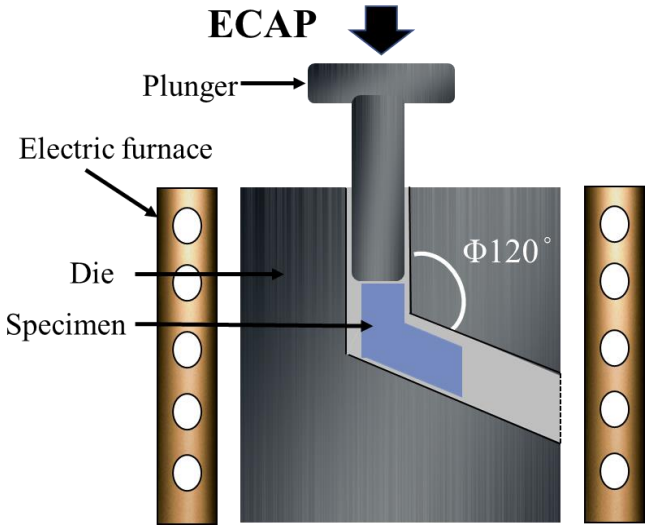

Figure 2. Equal Channel Angular Pressing (ECAP) setup with 120 degrees.

2.2. Microstructural Characterization

X-ray Diffraction (XRD) patterns were analyzed using the Bruker D2 PHASER X-ray (Germany) Diffractometer. Operating at 45 kV and 300W, the anode copper (Cu Kα) source provided detailed crystalline structure insights in the 20 to 80-degree range at a 0.04°/s scan rate. Subsequent data analysis was performed utilizing the Bruker EVA software. The obtained diffraction patterns were compared with the data from the Joint Committee of Powder Diffraction Standards (JCPDS) database, a widely recognized reference, to confirm the metallic phase composition and identify variations in diffraction planes.

Optical microscopy (OM) analysis was performed using the Zeiss Axiotech 25HD (Germany) microscope. Prior to observation, the material underwent meticulous sample preparation, including wet grinding with 4000-grit sandpaper and polishing with a mixture of 50 nm aluminum oxide powder and deionized water (1:5 ratio). The optimized surface preparation aimed to achieve a uniform and smooth sample for detailed optical examination. Subsequently, a suitable etchant was applied to unveil the metallographic features, as specified in Error! Reference source not found. (Emperor Chemical Co., Ltd. Taiwan). The microscope facilitated the detailed observation of macroscopic morphology, grain size, and defects.

Table 1. Etching solution combination.

Ethanol (ml)	DI water (ml)	Acetic Acid (ml)	Picric Acid (g)	Time (Sec)
100	10	5	6	25

 doi:10.20944/preprints202403.0603.v1

SEM analysis using the JEOL 7900F FE-SEM (Japan) provided a high-magnification observation of the material's surface morphology and microstructural features. Equipped with Energy Dispersive Spectrometry (EDS), it allowed comprehensive elemental analysis, enhancing understanding of the material's composition and distribution at the microscopic level.

2.3. Mechanical Characterization

Vickers hardness tester FR-1AN (Japan) with VHPro Express software, adhering to ASTM E18–94 standards was used to analyze the hardness of the AZ61 alloys. Using a 100gf load, the machine created a rhombic impression on the material's surface with a pyramidal diamond indenter (136° included angle) and an indentation duration of 10 seconds. Compression testing adhered to the ASTM E9 standard, utilizing specimens sized at 20×10×10 mm^3. The MTS-810 (United States) Compression Testing Machine was employed for the experiments. Each specimen underwent three compression tests, and the average values were calculated to determine the material's properties, including EL (%), YS (MPa), and UCS (MPa).

2.4. Corrosion Properties

The experiment adhered to ASTM B117 standards. A 72-hour salt spray test was con-ducted using deionized water containing 5% NaCl to induce corrosion behavior. The testing environment was maintained at a strict temperature of 35±0.5 ℃. Through meticulous observation and detailed corrosion area measurements, the study aimed to evaluate the material's corrosion resistance and performance under harsh environ-mental conditions.

3. Results

3.1. Phase Characterization

Figure 3 illustrates the X-ray diffraction (XRD) analysis of AZ61 alloy (Figure 3a) and AZ61+4wt.%Zn alloy (Figure 3b). XRD peaks corresponding to the α- $Mg_{0.97}Zn_{0.03}$ phase and β-$Mg_{17}Al_{12}$ phase is observed in both as-cast AZ61 and AZ61+4wt.%Zn. In the XRD patterns within the 2θ range of 30°– 45°, a noticeable decrease in the intensity of β-$Mg_{17}Al_{12}$ phase XRD peaks (411), (332) is observed after T4 heat treatment for both AZ61 and AZ61+4wt.%Zn alloys. Moreover, after undergoing ECAP with one pass, only the α - $Mg_{0.97}Zn_{0.03}$ phase was observed, indicating homogenization and complete dissolution of the β-$Mg_{17}Al_{12}$ phase during the ECAP process. These XRD results align with the observations from optical microscopy (OM) as depicted in Figure 4.

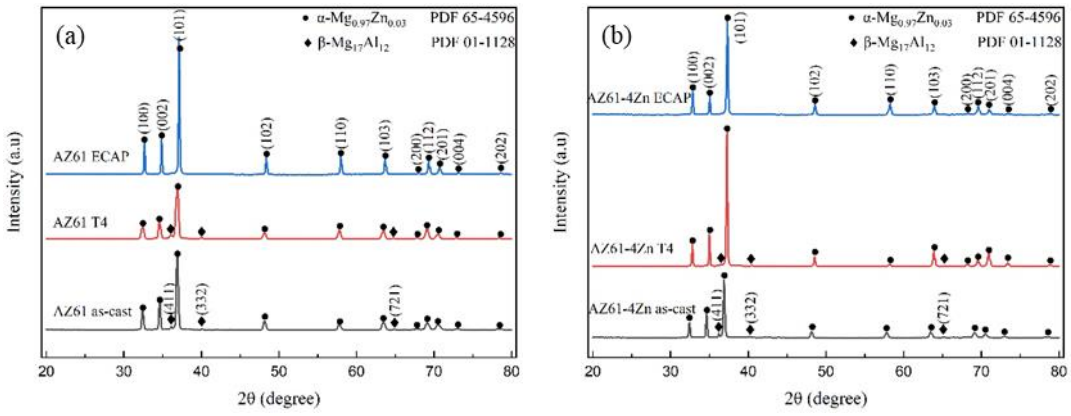

Figure 3. XRD analysis of fabricated (**a**) AZ61, (**b**) AZ61+4wt.%Zn.

 doi:10.20944/preprints202403.0603.v1

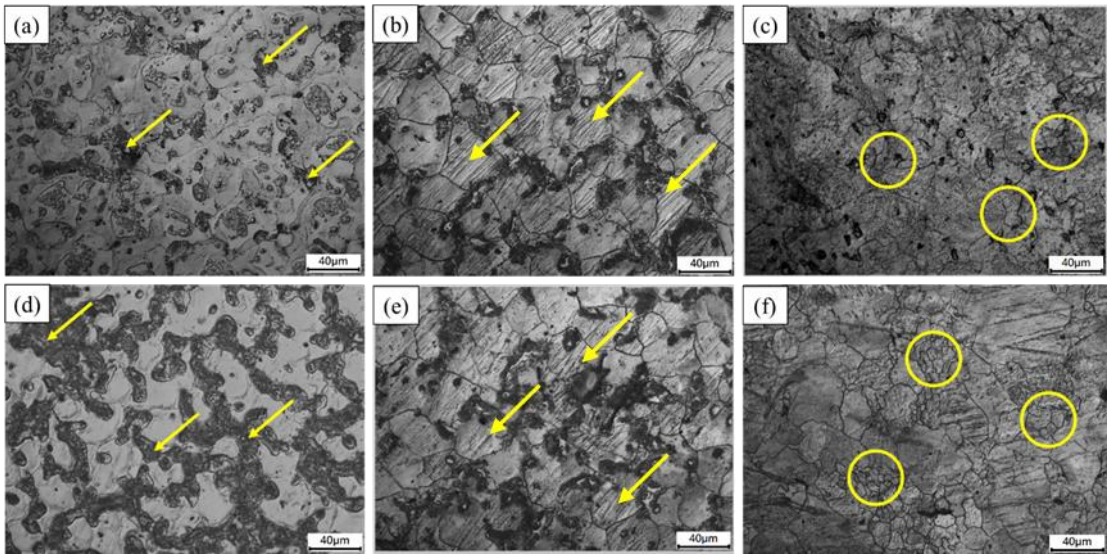

Figure 4. Optical microscopy microstructures of (**a**) AZ61-as-cast, (**b**) AZ61-T4, (**c**) AZ61-ECAP, (**d**) AZ61+4wt.%Zn-as-cast, (**e**) AZ61+4wt.%Zn-T4, (**f**) AZ61+4wt.%Zn-ECAP.

3.2. Microstructure Evaluation

The OM analysis of the as-cast, homogenized and ECAP-1 Pass AZ61 alloys are shown in Figure 4. Figure 4a,d depict the as-cast AZ61 and AZ61+4wt.%Zn, respectively. An increase in the second-phase area along the grain boundaries is observed with a 4 wt.% increase in zinc content (highlighted by yellow arrows), and the dispersion becomes more uniform. Figure 4b,e represents the AZ61 and AZ61+4wt.%Zn, after the homogenization treatment. It revealed that the most of the second phase has dissolved into the α-Mg matrix, but some remnants are still present along the grain boundaries. Figure 4c,f shows the AZ61 and AZ61+4wt.%Zn after 1 pass of ECAP. Compared to T4 homogenization conditions, the grain size of the samples subjected to ECAP is significantly re-fined, mainly attributed to the significant contribution of the dynamic recrystallization (DRX) mechanism. The sample with 4 wt.% zinc content shows a more pronounced grain refinement shown in Figure 4f (highlighted by yellow circles), with larger areas of extensive grain refinement and the generation of more fragmented small grains. As shown in Figure 6d after ECAP, the grain size reduces 70.17% in AZ61+4wt.%Zn.

Figure 5 presents the SEM analysis and EDS analysis of as-cast AZ61 (Figure 5a) and AZ61+4wt.%Zn (Figure 5b). The images indicate that the second phase in AZ61 without added zinc is mostly Mg-Al (highlighted by red arrows), forming clustered spherical shapes unevenly distributed. In contrast, AZ61+4wt.%Zn exhibits a Mg-Al-Zn second phase (highlighted by red arrows), presenting long and slender shapes uniformly distributed along the grain boundaries. These evenly distributed structures influence the ductility and strength of the composite material [24].

 doi:10.20944/preprints202403.0603.v1

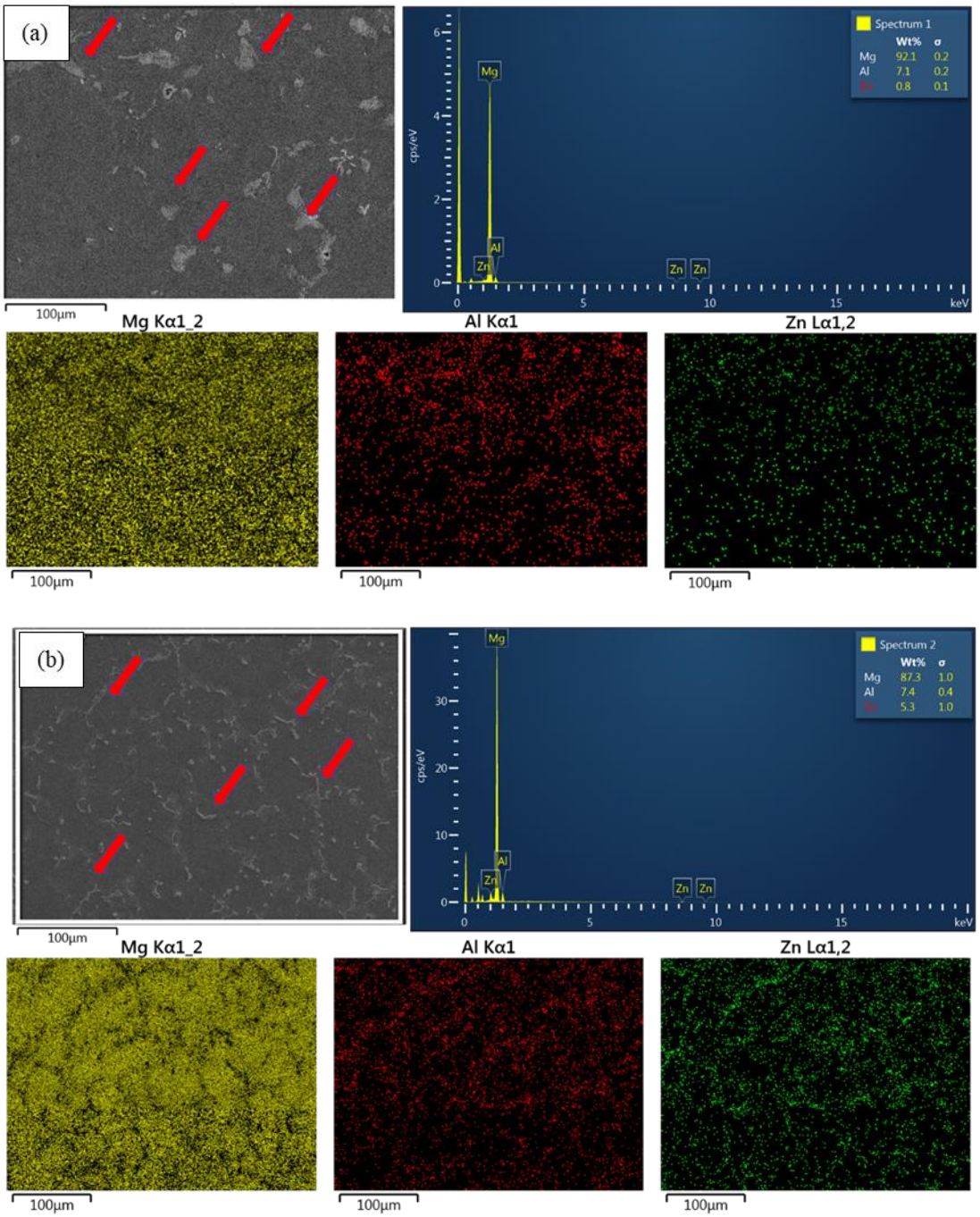

Figure 5. SEM microstructures and EDS elemental mapping study of (**a**) AZ61-as-cast, (**b**) AZ61+4wt.%Zn-as-cast.

 doi:10.20944/preprints202403.0603.v1

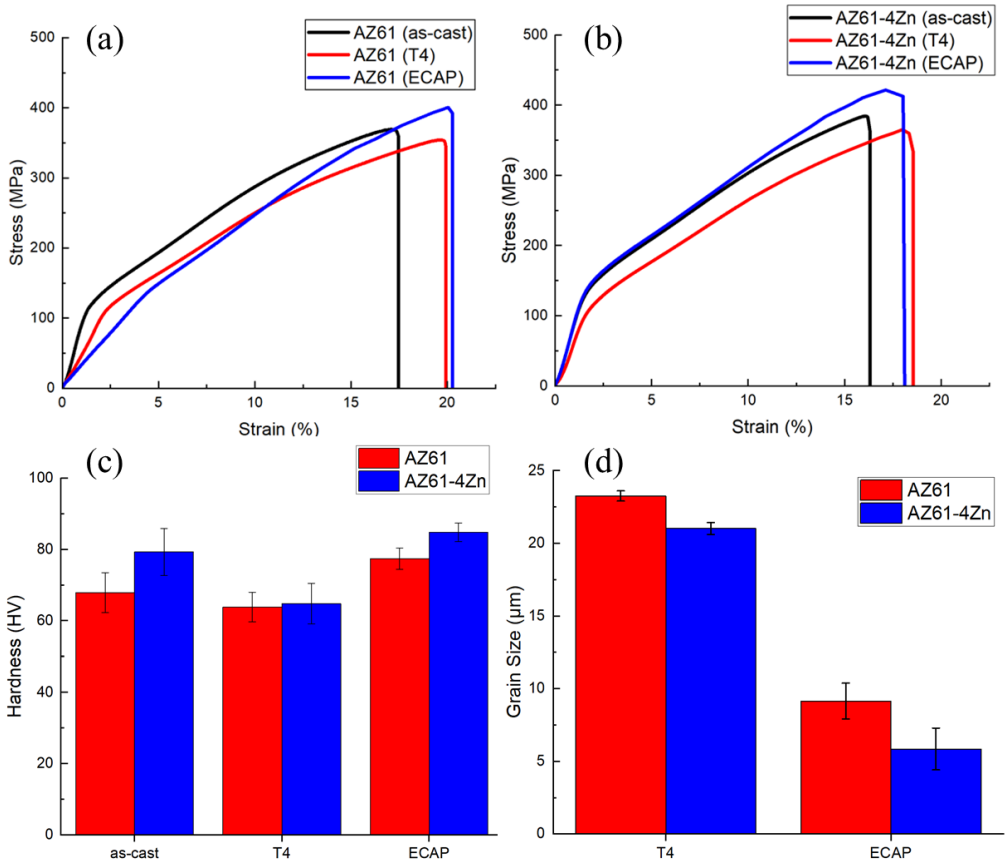

Figure 6. Stress–strain curves of (**a**) AZ61, (**b**) AZ61+4wt.%Zn, (**c**) Vickers hardness, (**d**) Average grain size.

3.3. Mechanical Properties

Stress-strain curves for AZ61 and AZ61+4wt.%Zn under as-cast, T4, and ECAP conditions are presented in Figure 6a,b. As indicated in Table 2, T4 homogenization treatment improves the EL of AZ61 by 13.32%, but YS and ultimate compression strength UCS decrease by 8.01% and 4.35%, respectively. After ECAP, the EL (22.96%), YS (141.53 MPa) and UCS (400.48 MPa) show significant improvements compared to as-cast, with increases of 19.19%, 13.51%, and 8.43%, respectively. For AZ61+4wt.%Zn, T4 treatment increases EL (19.19%), but YS (117.42 MPa) and UCS (365.43 MPa) decrease by 18.01% and 5.20%, respectively. After ECAP, AZ61+4wt.%Zn exhibits the best mechanical properties, with notable increases in EL (20.58%), YS (145.88 MPa), and UCS (421.79 MPa), representing improvements of 6.85%, 17.02%, and 14.19%, respectively.

Figure 6c and Table 2 demonstrate a slight decrease in hardness after T4 heat treatment for both materials, with AZ61+4wt.%Zn showing the most significant decrease of 22.39%. Figure 4d,e illustrates the substantial incorporation of the β-phase into the α-phase resulting from T4 heat treatment in AZ61+4wt.%Zn. After ECAP, the significant grain refinement (70.17%) in AZ61+4wt.%Zn, as shown in Figure 6d, leads to a hardness increase to 84.83 HV.

Table 2. A summary of the mechanical characteristics of the AZ61 and AZ61+4wt.%Zn alloy.

Composites	Process	EL (%)	YS (MPa)	UCS (MPa)	Hardness (HV)
AZ61	as-cast	19.26	124.67	369.36	67.88
	T4	21.83	115.42	353.97	63.87
	ECAP	22.96	141.53	400.48	77.44
AZ61+4wt.%Zn	as-cast	18.49	138.55	384.43	79.33
	T4	19.73	117.42	365.43	64.82
	ECAP	20.58	145.88	421.79	84.83

 doi:10.20944/preprints202403.0603.v1

3.4. Corrosion Properties

The results of salt spray tests are depicted in Figure 7. Figure 7a shows poor corrosion resistance on the surface of AZ61-as-cast, with uneven surface corrosion and numerous corroded pits (highlighted by yellow circles). Figure 7b,c displays the uneven corrosion on AZ61 after T4 heat treatment and ECAP. Figure 7d–f show specimens of AZ61+4wt.%Zn after different processing steps. With the addition of 4wt.% Zn, the corrosion area becomes more uniform, with only a few corroded pits observed in Figure 7d AZ61+4wt.%Zn-as-cast. The best corrosion resistance is observed in Figure 7f for AZ61+4wt.%Zn after ECAP, with a majority of the surface remaining uncorroded and exhibiting a bright appearance.

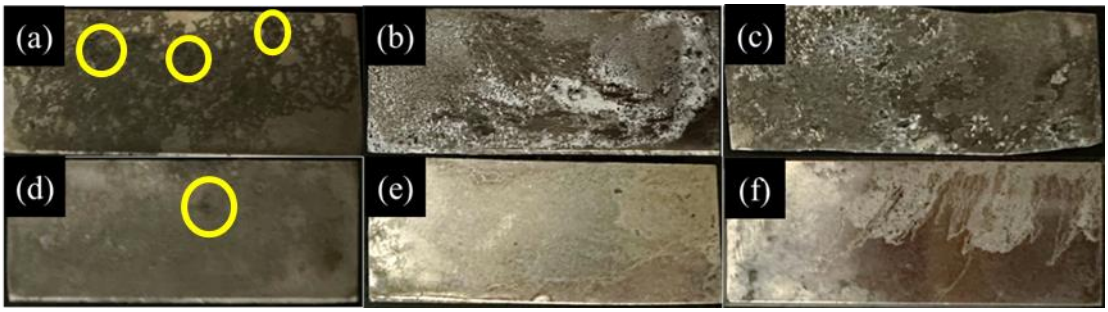

Figure 7. Surface morphology of salt spray treated samples (**a**) AZ61-as-cast, (**b**) AZ61-T4, (**c**) AZ61-ECAP, (**d**) AZ61+4wt.%Zn-as-cast, (**e**) AZ61+4wt.%Zn-T4, (**f**) AZ61+4wt.%Zn-ECAP.

4. Discussion

In this study, the influence of zinc addition and secondary processing on the mechanical properties of the AZ61 magnesium alloy has been thoroughly investigated. The initial observations revealed the presence of aluminum (Al) in the form of β-$Mg_{17}Al_{12}$ precipitates within the magnesium alloy matrix [25,26], as illustrated in Figure 4a. During the homogenization process, an increase in temperature led to an enhanced solubility of aluminum in the magnesium matrix. The β-$Mg_{17}Al_{12}$ phase was observed at grain boundaries, eventually dissolving into the α-Mg supersaturated solid solution and cooling in the form of fine particles [27]. The second phase significantly affects the mechanical and corrosion properties of magnesium alloy [28], as confirmed by the findings presented in Figure 5b.

The addition of 4wt.% zinc, as depicted in Figure 5b, induced structural modifications in the magnesium alloy, impacting the lattice structure and solid solubility [29]. This transformation resulted in a shift from coarse to elongated structures and a more uniform distribution of the second phase [30]. This phenomenon significantly influenced the alloy's mechanical performance, corrosion resistance, and other properties, as evidenced in Table 2.

Upon subjecting the alloy to T4 heat treatment, dual grain structures were observed, as indicated by yellow arrows in Figure 4b,e. The heat treatment process led to recrystallization or growth of grains, with the formation of dual grain structures due to uneven growth rates in different directions during solidification [31]. Additionally, the presence of impurity cores within the material during heat treatment possibly guided grain orientation, contributing to the observed dual grain structures [23]. T4 heat treatment adversely affected the mechanical properties of the AZ61 magnesium alloy, resulting in a decrease in both strength and hardness, as outlined in Table 2.

The strength behavior of materials processed through Severe Plastic Deformation (SPD), such as Equal Channel Angular Pressing (ECAP), is primarily influenced by grain size, dislocation density, and crystallographic texture [32–34]. The reduction in grain size, as illustrated in Figure 6d, post-ECAP processing of AZ61+4wt.%Zn, demonstrated a pronounced grain refinement effect, effectively enhancing mechanical strength. The improved strength can be attributed to Orowan strengthening and the load-carrying effect [35]. The heat treatment performed during the ECAP process facilitated the complete dissolution of β-$Mg_{17}Al_{12}$ into the α phase, as shown in Figure 4c,f, contributing to the enhancement of material mechanical properties.

 doi:10.20944/preprints202403.0603.v1

The hardness test results in Figure 6c align with the research conducted by S.J Huang et al. work [36]. The authors investigated the impact of ECAP on grain refinement in AZ61 Mg alloys, demonstrating that an increase in the number of ECAP passes leads to a reduction in average grain size, accompanied by an increase in both hardness and ductility. Therefore, the observed hardness outcomes may be attributed to grain refinement, the size of hard phase particles, and strain hardening during the ECAP process.

This study explored the impact of the presence, morphology, and distribution of the second phase in magnesium alloys on corrosion resistance (Figure 7). Post-ECAP treatment, AZ61+4wt.%Zn exhibited increased corrosion resistance, potentially associated with the size and distribution of second-phase particles [30]. The transformation of large, coarse second-phase particles to smaller sizes and a more uniform distribution after ECAP treatment was crucial for improved corrosion resistance [37]. The role of ECAP in influencing these microstructural features, especially the small and uniformly distributed second phase, proved essential in mitigating the micro galvanic effect. Moreover, the significant reduction in grain size compared to cast alloy further enhanced corrosion resistance (Figure 4f).

In conclusion, our study highlights the efficiency of alloying element addition and secondary processing in tuning the microstructure of magnesium alloys, leading to improved mechanical performance and corrosion resistance. The findings underscore the potential for tailoring magnesium alloy properties for specific applications through controlled alloying and processing techniques.

5. Conclusions

In this research, the stir casting method was employed to fabricate AZ61 and AZ61+4wt.%Zn magnesium alloy. The influence of equal channel angular pressing (ECAP) on the microstructure, mechanical properties, and corrosion resistance of the materials was thoroughly investigated. The key findings and conclusions are summarized as follows:

(1) Microstructural analysis revealed that the addition of 4wt.% Zn resulted in a significant refinement of β-$Mg_{17}Al_{12}$ phases, uniformly distributed along the grain boundaries. This refinement was further enhanced after ECAP processing, leading to a more pronounced grain refinement in AZ61+4wt.%Zn. This refinement played a crucial role in the notable improvement of mechanical and corrosion properties.

(2) The region with the most extensive Dynamic Recrystallization (DRX) grain refinement was observed in AZ61+4wt.%Zn after ECAP processing, showcasing the highest yield strength (145.88 MPa), ultimate compression strength (421.79 MPa), and hardness (84.83 HV).

(3) T4 heat treatment demonstrated a significant impact on the solid solution of β-$Mg_{17}Al_{12}$ in Mg-Al alloys. Both AZ61 and AZ61+4wt.%Zn exhibited increased elongation rates by 13.32% and 19.19%, respectively, after T4 heat treatment.

(4) ECAP has been demonstrated as an effective method for enhancing the mechanical properties and corrosion resistance of magnesium alloys. The results indicate that ECAP has increased the mechanical properties of AZ61+4wt.%Zn, showing improvements of 6.85% in EL, 17.02% in YS, and 14.19% in UCS. Furthermore, with regard to corrosion properties, ECAP significantly reduces the corrosion rate and promotes a more uniform corrosion surface.

Author Contributions: Conceptualization, S.-J.H., validation, S.-J.H. and S.-Y.W.; formal analysis, S.-J.H., S.-Y.W. and M.S.; resources, S.-Y.W. and M.S.; writing—original draft preparation, S.-Y.W. and M.S.; writing—review and editing, S.-J.H. and S.-Y.W.; visualization, S.-Y.W. and M.S.; supervision, S.-J.H.; All authors have read and agreed to the published version of the manuscript.

Funding: This research was funded by The Ministry of Science and Technology, Taiwan (NSTC111-2221-E-011-096-MY3), for providing financial support..

Institutional Review Board Statement: Not applicable.

Informed Consent Statement: Not applicable.

Data Availability Statement: The data presented in this study are available in the article.

Acknowledgments: The authors would like to thank the Ministry of Science and Technology, Taiwan for providing financial support..

Conflicts of Interest: The authors declare no conflict of interest.

References

1. Han, G.; Lu, Y.; Jia, H.; Ding, Z.; Wu, L.; Shi, Y.; Wang, G.; Luo, Q.; Chen, Y.; Wang, J.; et al. Magnesium-Based Energy Materials: Progress, Challenges, and Perspectives. Journal of Magnesium and Alloys 2023, 11, 3896–3925, doi:10.1016/j.jma.2023.08.009.
2. Balasubramani, N.; Wang, G.; Easton, M.A.; StJohn, D.H.; Dargusch, M.S. A Comparative Study of the Role of Solute, Potent Particles and Ultrasonic Treatment during Solidification of Pure Mg, Mg–Zn and Mg–Zr Alloys. Journal of Magnesium and Alloys 2021, 9, 829–839, doi:10.1016/j.jma.2020.08.006.
3. Osipenko, M.A.; Kharytonau, D.S.; Kasach, A.A.; Ryl, J.; Adamiec, J.; Kurilo, I.I. Inhibitive Effect of Sodium Molybdate on Corrosion of AZ31 Magnesium Alloy in Chloride Solutions. Electrochim Acta 2022, 414, 140175, doi:10.1016/j.electacta.2022.140175.
4. Zhu, X.; Liu, F.; Wang, S.; Ji, S. The Development of Low-Temperature Heat-Treatable High-Pressure Die-Cast Al–Mg–Fe–Mn Alloys with Zn. J Mater Sci 2021, 56, 11083–11097, doi:10.1007/s10853-021-05972-5.
5. Kumar, D.; Phanden, R.K.; Thakur, L. A Review on Environment Friendly and Lightweight Magnesium-Based Metal Matrix Composites and Alloys. Mater Today Proc 2021, 38, 359–364, doi:10.1016/j.matpr.2020.07.424.
6. Gneiger, S.; Papenberg, N.; Mitsche, S.; Fehlbier, M. Manufacturing and Processing of Sheets Using a Mg–Al–Ca–Zn–Y Alloy for Automotive Applications. Results in Engineering 2024, 21, 101700, doi:10.1016/j.rineng.2023.101700.
7. Esmaily, M.; Svensson, J.E.; Fajardo, S.; Birbilis, N.; Frankel, G.S.; Virtanen, S.; Arrabal, R.; Thomas, S.; Johansson, L.G. Fundamentals and Advances in Magnesium Alloy Corrosion. Prog Mater Sci 2017, 89, 92–193, doi:10.1016/j.pmatsci.2017.04.011.
8. Olugbade, T.O.; Omiyale, B.O.; Ojo, O.T. Corrosion, Corrosion Fatigue, and Protection of Magnesium Alloys: Mechanisms, Measurements, and Mitigation. J Mater Eng Perform 2022, 31, 1707–1727, doi:10.1007/s11665-021-06355-2.
9. Nie, K.B.; Deng, K.K.; Wang, X.J.; Wang, T.; Wu, K. Influence of SiC Nanoparticles Addition on the Microstructural Evolution and Mechanical Properties of AZ91 Alloy during Isothermal Multidirectional Forging. Mater Charact 2017, 124, 14–24, doi:10.1016/j.matchar.2016.12.006.
10. Liu, B.; Yang, J.; Zhang, X.; Yang, Q.; Zhang, J.; Li, X. Development and Application of Magnesium Alloy Parts for Automotive OEMs: A Review. Journal of Magnesium and Alloys 2023, 11, 15–47, doi:10.1016/j.jma.2022.12.015.
11. Wellbrock, W.; Ludin, D.; Röhrle, L.; Gerstlberger, W. Sustainability in the Automotive Industry, Importance of and Impact on Automobile Interior – Insights from an Empirical Survey. International Journal of Corporate Social Responsibility 2020, 5, 10, doi:10.1186/s40991-020-00057-z.
12. Zhang, W.; Xu, J. Advanced Lightweight Materials for Automobiles: A Review. Mater Des 2022, 221, 110994, doi:10.1016/j.matdes.2022.110994.
13. Manjhi, S.K.; Sekar, P.; Bontha, S.; Balan, A.S.S. Additive Manufacturing of Magnesium Alloys: Characterization and Post-Processing. International Journal of Lightweight Materials and Manufacture 2024, 7, 184–213, doi:10.1016/j.ijlmm.2023.06.004.
14. Naseri, M.; Moghadam, A.O.; Anandkumar, M.; Sudarsan, S.; Bodrov, E.; Samodurova, M.; Trofimov, E. Enhancing the Mechanical Properties of High-Entropy Alloys through Severe Plastic Deformation: A Review. Journal of Alloys and Metallurgical Systems 2024, 5, 100054, doi:10.1016/j.jalmes.2024.100054.
15. Ebrahimi, M.; Attarilar, S.; Gode, C.; Kandavalli, S.R.; Shamsborhan, M.; Wang, Q. Conceptual Analysis on Severe Plastic Deformation Processes of Shape Memory Alloys: Mechanical Properties and Microstructure Characterization. Metals (Basel) 2023, 13, 447, doi:10.3390/met13030447.
16. Description of Severe Plastic Deformation (SPD). In Bulk Nanostructured Materials; Wiley, 2013; pp. 6–21.
17. Muralidhar, A.; Narendranath, S.; Shivananda Nayaka, H. Effect of Equal Channel Angular Pressing on AZ31 Wrought Magnesium Alloys. Journal of Magnesium and Alloys 2013, 1, 336–340, doi:10.1016/j.jma.2013.11.007.
18. Tan, Y.; Li, W.; Hu, W.; Shi, X.; Tian, L. The Effect of ECAP Temperature on the Microstructure and Properties of a Rolled Rare Earth Magnesium Alloy. Materials 2019, 12, 1554, doi:10.3390/ma12091554.
19. Prasad, S.V.S.; Prasad, S.B.; Verma, K.; Mishra, R.K.; Kumar, V.; Singh, S. The Role and Significance of Magnesium in Modern Day Research-A Review. Journal of Magnesium and Alloys 2022, 10, 1–61, doi:10.1016/j.jma.2021.05.012.

20. Bryła, K.; Horky, J. Magnesium Alloys Processed by Severe Plastic Deformation (SPD) for Biomedical Applications: An Overview. Mater Trans 2023, 64, MT-MF2022056, doi:10.2320/matertrans.MT-MF2022056.
21. Wang, X.; Brünger, E.; Gottstein, G. Microstructure Characterization and Dynamic Recrystallization in an Alloy 800H. Materials Science and Engineering: A 2000, 290, 180–185, doi:10.1016/S0921-5093(00)00915-1.
22. Abbas, A.; Huang, S.-J. Investigating the Synergic Effects of WS2 and ECAP on Degradation Behavior of AZ91 Magnesium Alloy. Coatings 2022, 12, 1710, doi:10.3390/coatings12111710.
23. Huang, S.-J.; Subramani, M.; Borodianskiy, K.; Immanuel, P.N.; Chiang, C.-C. Effect of Equal Channel Angular Pressing on the Mechanical Properties of Homogenized Hybrid AZ61 Magnesium Composites. Mater Today Commun 2023, 34, 104974, doi:10.1016/j.mtcomm.2022.104974.
24. Zan, Y.N.; Zhou, Y.T.; Liu, Z.Y.; Ma, G.N.; Wang, D.; Wang, Q.Z.; Wang, W.G.; Xiao, B.L.; Ma, Z.Y. Enhancing Strength and Ductility Synergy through Heterogeneous Structure Design in Nanoscale Al2O3 Particulate Reinforced Al Composites. Mater Des 2019, 166, 107629, doi:10.1016/j.matdes.2019.107629.
25. Li, Y.; Tan, C.; Yu, X.; Nie, Z.; Zhao, X.; Han, J.; Yuan, S.; Zhao, M.; Guo, C.; Wang, F. Evolution of β Mg17Al12 in Mg Al Zn Ag Alloy over Time. Materials Science and Engineering: A 2019, 754, 470–478, doi:10.1016/j.msea.2019.03.094.
26. Huang, S.-J.; Subramani, M.; Ali, A.N.; Alemayehu, D.B.; Aoh, J.-N.; Lin, P.-C. The Effect of Micro-SiCp Content on the Tensile and Fatigue Behavior of AZ61 Magnesium Alloy Matrix Composites. International Journal of Metalcasting 2021, 15, 780–793, doi:10.1007/s40962-020-00508-0.
27. Elambharathi, B.; Kumar, S.D.; Dhanoop, V.U.; Dinakar, S.; Rajumar, S.; Sharma, S.; Kumar, V.; Li, C.; Eldin, E.M.T.; Wojciechowski, S. Novel Insights on Different Treatment of Magnesium Alloys: A Critical Review. Heliyon 2022, 8, e11712, doi:10.1016/j.heliyon.2022.e11712.
28. Dai, C.; Wang, J.; Pan, Y.; Ma, K.; Peng, Y.; Ren, J.; Wang, Y.; Wang, D.; Wang, J.; Ma, Y. Tailoring the Microstructural Characteristic and Improving the Corrosion Rate of Mg-Gd-Ni Alloy by Heat Treatment with Different Volume Fraction of LPSO Phase. Corros Sci 2023, 210, 110806, doi:10.1016/j.corsci.2022.110806.
29. Sharma, S.K.; Saxena, K.K.; Malik, V.; Mohammed, K.A.; Prakash, C.; Buddhi, D.; Dixit, S. Significance of Alloying Elements on the Mechanical Characteristics of Mg-Based Materials for Biomedical Applications. Crystals (Basel) 2022, 12, 1138, doi:10.3390/cryst12081138.
30. Asadollahi, M.; Gerashi, E.; Alizadeh, R.; Mahmudi, R. Effect of Zn Content and Processing Route on the Microstructure, Mechanical Properties, and Bio-Degradation of Mg–Zn Alloys. Journal of Materials Research and Technology 2022, 21, 4473–4489, doi:10.1016/j.jmrt.2022.11.041.
31. Ye, X.; Suo, Z.; Heng, Z.; Chen, B.; Wei, Q.; Umeda, J.; Kondoh, K.; Shen, J. An In-Situ Study of Static Recrystallization in Mg Using High Temperature EBSD. Journal of Magnesium and Alloys 2023, doi:10.1016/j.jma.2023.01.021.
32. Liu, F.; Chen, X.; Zhao, Y.; Wang, W.; Zou, D.; Li, R.; Xiong, X.; Su, B. Effects of Severe Plastic Deformation on the Microstructures, Mechanical Properties, and Corrosion Behavior of U-5.5Nb Alloy. Journal of Nuclear Materials 2021, 557, 153274, doi:10.1016/j.jnucmat.2021.153274.
33. Bhat K, U.; Bhat Panemangalore, D.; Bhat, S. Equal Channel Angular Processing—a Modern Deforming Technique for Quality Products. In Advanced Welding and Deforming; Elsevier, 2021; pp. 381–423.
34. Kapoor, R. Severe Plastic Deformation of Materials. In Materials Under Extreme Conditions; Elsevier, 2017; pp. 717–754.
35. Zhang, Z.; Chen, D.L. Contribution of Orowan Strengthening Effect in Particulate-Reinforced Metal Matrix Nanocomposites. Materials Science and Engineering: A 2008, 483–484, 148–152, doi:10.1016/j.msea.2006.10.184.
36. Huang, S.-J.; Subramani, M.; Borodianskiy, K. Strength and Ductility Enhancement of AZ61/Al2O3/SiC Hybrid Composite by ECAP Processing. Mater Today Commun 2022, 31, 103261, doi:10.1016/j.mtcomm.2022.103261.
37. Hashemi, M.; Alizadeh, R.; Langdon, T.G. Recent Advances Using Equal-Channel Angular Pressing to Improve the Properties of Biodegradable Mg–Zn Alloys. Journal of Magnesium and Alloys 2023, 11, 2260–2284, doi:10.1016/j.jma.2023.07.009.